

# MGT-Prism: Enhancing Domain Generalization for Machine-Generated Text Detection via Spectral Alignment

Shengchao Liu<sup>1</sup>, Xiaoming Liu<sup>1,\*</sup>, Chengzhengxu Li<sup>1</sup>,  
 Zhaohan Zhang<sup>2</sup>, Guoxin Ma<sup>1</sup>, Yu Lan<sup>1</sup>, Shuai Xiao<sup>3</sup>

<sup>1</sup>Faculty of Electronic and Information Engineering, Xi'an Jiaotong University

<sup>2</sup>Queen Mary University of London, <sup>3</sup>Alibaba

{liusc, czx.li, guoxin.ma}@stu.xjtu.edu.cn, zhaohan.zhang@qmul.ac.uk  
 {xm.liu, ylan2020}@xjtu.edu.cn, shuai.xsh@alibaba-inc.com

## Abstract

Large Language Models have shown growing ability to generate fluent and coherent texts that are highly similar to the writing style of humans. Current detectors for Machine-Generated Text (MGT) perform well when they are trained and tested in the same domain but generalize poorly to unseen domains, due to domain shift between data from different sources. In this work, we propose MGT-Prism, an MGT detection method from the perspective of the frequency domain for better domain generalization. Our key insight stems from analyzing text representations in the frequency domain, where we observe consistent spectral patterns across diverse domains, while significant discrepancies in magnitude emerge between MGT and human-written texts (HWTs). The observation initiates the design of a low frequency domain filtering module for filtering out the document-level features that are sensitive to domain shift, and a dynamic spectrum alignment strategy to extract the task-specific and domain-invariant features for improving the detector's performance in domain generalization. Extensive experiments demonstrate that MGT-Prism outperforms state-of-the-art baselines by an average of 0.90% in accuracy and 0.92% in F1 score on 11 test datasets across three domain-generalization scenarios.

## 1 Introduction

Large Language Models (LLMs) are becoming popular as writing assistants in daily work for their incredible ability to generate fluent and coherent texts following users' instructions. However, the widespread applications of LLMs have raised substantial concerns regarding their misuse in fake news generation (Liu et al., 2024a), ghostwriting (Kumar et al., 2025), spamming, etc. (Wang et al., 2024; Li et al., 2025b; Zellers et al., 2019; Pudasaini et al., 2025), which calls for an urgent need to detect MGTs precisely and reliably.

\*Corresponding author

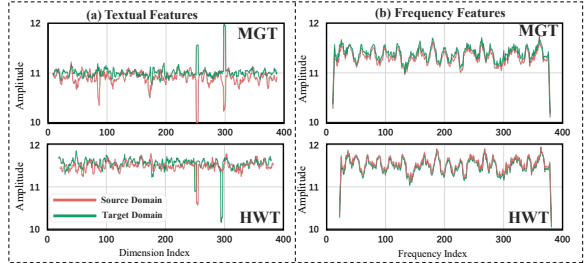


Figure 1: **Comparison of the textual features and their corresponding frequency features.** The horizontal axis represents the feature dimension index for both textual and frequency-domain features, while the vertical axis shows the magnitude of raw feature values in the text domain and transformed frequency components, respectively. Frequency features exhibit more consistent patterns between intra-class samples from different domains, providing the foundation for frequency-based detection under domain shift<sup>1</sup>.

Due to the diversity in application scenarios, model architectures, and scales of LLMs, an ideal MGT detector should perform consistently well in *domain generalization*<sup>2</sup> (DG) settings where the detector is trained on datasets from different source domains and tested on unseen target domains. Two mainstream approaches dominate current MGT detection methods, *i.e.*, fine-tuning and metrics-based methods, yet both largely neglect the detector's ability to generalize. Existing fine-tuning methods either focus on capturing distinguishing features between MGT and HWT, such as text coherence (Liu et al., 2023), token probabilities (Chen et al., 2025; Bao et al., 2023; Wang et al., 2023a), and attention patterns (Kushnareva et al., 2021), or explore novel training strategies, including contrastive learning (Liu et al., 2024b), and adversarial

<sup>1</sup>The data used in our experiments consist of 3,000 randomly sampled HWTs and 3,000 MGTs from both the source and target domains, covering all three datasets used in domain generalization.

<sup>2</sup>In this work, we use *domain generalization* to refer to generalization across MGT domains, MGT generators, and generator scales in MGT detection.

training (Hu et al., 2023; Li et al., 2025b). However, these methods do not explicitly disentangle task-specific and domain-specific features during training, resulting in limited domain generalization. Metric-based methods work in an unsupervised manner. They calculate a single score for distinguishing MGTs from HWTs using perplexity (Bao et al., 2024), entropy (Shum et al., 2023), or resampling (Shi et al., 2024). Metric-based methods also suffer from performance degradation in DG settings, as they rely on a specific training set for deciding the optimized classification threshold.

Inspired by the potential of the frequency domain to disentangle the feature representations into orthogonal components (Tamkin et al., 2020a; Sun et al., 2024; Guo et al., 2023), we examine the inter- and intra-class features from the perspective of spectra using Discrete Fourier Transform (DFT) (Bracewell, 1986). The preliminary analysis in Sec. 3 reveals a critical property of text representations in the frequency domain. As shown in Figure 1, the spectrum of intra-class text representation from different domains exhibits differences in the magnitude but is more consistent in the distribution pattern, indicating that *i*) distinguishable features between MGT and HWT exist in the frequency domain; *ii*) transfer from features space to frequency domain mitigates the domain shift.

Based on the natures of spectra, which are decomposability and insensitivity to domain shift, we propose MGT-Prism, an MGT detection framework from the perspective of the frequency domain, to align intra-class features from different domains for emphasizing the task-specific and domain-invariant inter-class features, therefore enabling strong DG ability of MGT detectors. Specifically, we design a frequency spectrum filter block to suppress domain-related features (Tamkin et al., 2020a). To mitigate the domain shift in finer-grain, we further introduce a frequency spectrum alignment strategy to reduce the distribution discrepancy among intra-class instances in the frequency domain. By aligning intra-class features in the frequency domain, MGT-Prism successfully extracts and utilizes the task-specific and domain-invariant features from the training set and generalizes well to unseen domains. Extensive experiments demonstrate the strong generalization ability of MGT-Prism among multiple settings. Compared to state-of-the-art approaches in accuracy and F1 score, MGT-Prism achieves average improvements of 0.92% and 1.56%, 0.90% and

0.69%, and 0.88% and 1.24% in cross-generator, cross-domain, and cross-scale, respectively, highlighting its efficacy. Our contributions are summarized as follows:

- We propose to analyze MGT detection in the frequency domain and observe a similar distribution pattern with varied magnitudes between MGT and HWT spectra, offering a new insight and broad applicability in MGT detection.
- We design a novel model, MGT-Prism, which aligns the intra-class features in text spectra from different domains to extract task-specific and domain-invariant features for enhancing domain generalizability in MGT detection.
- We conduct extensive experiments on 11 test sets across three generalization scenarios. The results demonstrate that our model consistently outperforms state-of-the-art methods in both effectiveness and generalization capability for MGT detection.

## 2 Related Work

**Domain Generalization.** In the context of MGT detection, DG means a detector should remain reliable when faced with text from new generators or domains not encountered during training. Many metric-based detectors rely on head-token analysis (Gehrmann et al., 2019), logistic regression on perplexity features (Bao et al., 2024, 2023), or token-wise log probabilities (Wang et al., 2023b; Hans et al., 2024) from white-box LLMs to address this challenge. While metric-based methods are training-free, their prediction accuracy is often lower than supervised approaches. In contrast, fine-tuned detectors benefit from perturbation-based methods (Li et al., 2025a; Gao et al., 2022; Shum et al., 2023), contrastive learning (Tack et al., 2020; Gunel et al., 2021), or a combination of both (Liu et al., 2024a), which have proven effective in improving model generalization. In addition, adversarial training frameworks (Li et al., 2025b; Hu et al., 2023) have been employed to address robustness issues. Unlike prior methods based on overall text features, our approach introduces the Fourier Transform to extract multi-scale frequency information, emphasizing both global and local patterns, and mitigates distributional bias to enable effective detection in DG.

**Fourier Transforms.** Recently, frequency-based techniques have been increasingly integrated into the computer vision field (Yue et al., 2025; Yi et al., 2023; Guo et al., 2023). By analyzing how low frequencies in an image typically capture global structures (Fan et al., 2022) and color information (Cao et al., 2020), while high frequencies contain fine details of objects, a series of methods to enhance predictive capabilities have emerged (Woo et al., 2022; Fan et al., 2022). Some works have applied these techniques to the natural language processing (NLP) field (Wu et al., 2021; Lee-Thorp et al., 2021), combining them with attention mechanisms to accelerate computations (Tamkin et al., 2020a; Lee-Thorp et al., 2021; Choromanski et al., 2020), and embedding spectral filters in different tasks (Fang and Xu, 2024; Tamkin et al., 2020a; Khan et al., 2019; Rippel et al., 2015), where the low-frequency components are considered to represent slower-changing features. Inspired by this, we observe that transforming representations from the feature space to the frequency domain reduces dimensional complexity. It also enhances the structural regularity of feature distributions in frequency domain. This transformation amplifies distributional irregularities (e.g., lexical repetition, unnatural conjunctions, and templated phrasing), making MGT and HWT more distinguishable for downstream detection.

### 3 Preliminary

This section briefly introduces the problem formulation and the Discrete Fourier Transform (DFT) in traditional signal processing and its application in our work.

#### 3.1 MGT Detection under DG

The DG task is defined as follows: given a training set consisting of multiple observed source domains  $\mathcal{D}_S = \{\mathcal{D}_n\}_{n=1}^N$ , where each domain  $\mathcal{D}_n = \{(x_i^{(n)}, y_i^{(n)})\}_{i=1}^{T_n}$  contains  $T_n$  labeled samples, the goal is to learn a model from  $\mathcal{D}_S$  that generalizes to arbitrary unseen target domains  $\mathcal{D}_T$  whose distributions differ from those of the sources.

#### 3.2 Discrete Fourier Transform

The Continuous Fourier Transform (CFT) is one of the core mathematical tools in the field of signal processing (Bracewell, 1986). The idea is that any complex signal can be decomposed into a superposition of sine waves (or complex exponen-

tials) of different frequencies. Specifically, for any time-domain signal  $x(t)$ , its frequency component  $X(f)$  at frequency  $f$  in the frequency domain is expressed as:

$$X(f) = \int_{-\infty}^{\infty} x(t)e^{-2\pi jft} dt, \quad (1)$$

where  $e^{-2\pi jft}$  is the complex exponential basis and  $j$  denotes the imaginary unit. The DFT extends the CFT to discrete signals, where  $x[n]$  denotes uniformly sampled values of  $x(t)$ . The  $k$ -th frequency component in the frequency domain is:

$$X[k] = \sum_{n=0}^{N-1} x[n]e^{-2\pi j \frac{kn}{N}}, \quad 0 \leq k \leq (N-1), \quad (2)$$

where  $N$  represents the length of the signal, which is the number of sampling points of the input sequence  $x[n]$ .

#### 3.3 Applying DFT to Contextual Word Representations

Given an input sequence  $x[n]$ , an encoder-only Transformer (e.g., RoBERTa) produces final-layer token vectors  $V = (v_0, \dots, v_{N-1})$ , where  $v_t \in \mathbb{R}^d$ . Fix a neuron  $i \in \{0, \dots, d-1\}$  and consider its trajectory across tokens  $s^{(i)} = (v_0[i], \dots, v_{N-1}[i]) \in \mathbb{R}^N$ . Building on Eq. (2), which treats the final-layer [CLS] vector as a length- $d$  signal along the hidden dimension, we generalize to the token axis: fixing neuron  $i$ , we apply the same DFT to its activations across tokens  $s^{(i)}$ . The spectral coefficients  $h_k^{(i)}$  are:

$$h_k^{(i)} = \sum_{t=0}^{N-1} s_t^{(i)} e^{-2\pi i k t / N}, \quad k = 0, \dots, N-1. \quad (3)$$

Here  $k = 0$  is the lowest component (Direct Current component). Low-, high-, or band-pass effects are obtained by applying a spectral mask  $m_k$  (e.g., zeroing selected  $h_k^{(i)}$ ).

#### 3.4 Why Frequency Helps MGT Detection Generalize Across Domains

A common property of modern NLP models is their ability to produce *contextualized* token representations by modeling a sequence of tokens (e.g., characters or subword units). We collect the frequency-domain features as  $\mathbf{H} = \{\mathbf{h}_k\}_{k=0}^{N-1}$ , where  $\mathbf{h}_k = [h_k^{(0)}, \dots, h_k^{(d-1)}]^\top$ . To capture global

structural patterns, we keep components that complete at most one full oscillation over the input. Consequently, we define the low-frequency band as:

$$\mathbf{H}_{\text{low}} = \{\mathbf{h}_k\}_{k=0}^{d_{\text{low}}}, \quad d_{\text{low}} = \left\lceil \frac{N}{t_{\text{num}}} \right\rceil. \quad (4)$$

where  $t_{\text{num}}$  is the number of tokens in the input text. Similarly, to capture sentence-level features, we retain components with at most one oscillation per sentence, based on the sentence count  $s_{\text{num}}$ :

$$\mathbf{H}_{\text{mid}} = \{\mathbf{h}_k\}_{k=d_{\text{low}}+1}^{d_{\text{mid}}}, \quad d_{\text{mid}} = \left\lceil \frac{N}{s_{\text{num}}} + (N - d_{\text{low}}) \right\rceil. \quad (5)$$

After obtaining the mid frequency band  $\mathbf{H}_{\text{mid}}$ , we divide the remaining frequency features into high frequency band:

$$\mathbf{H}_{\text{high}} = \{\mathbf{h}_k\}_{k=d_{\text{mid}}+1}^{N-1}. \quad (6)$$

The inverse DFT (IDFT; Lee-Thorp et al. (2021)), which transforms the input from the frequency domain  $\mathbf{H}_f$  back to the text feature space  $H_f$ , can be expressed as:

$$H_f = \text{IDFT}(\mathbf{H}_f) \quad (7)$$

Previous studies (Tamkin et al., 2020b) have shown that the high-frequency components reflect word-level features (e.g., perplexity, log-probability), while low-frequency components are associated with document-level characteristics (e.g., topic, style). Correspondingly, recent studies Detect-GPT (Mitchell et al., 2023) and Binoculars (Hans et al., 2024) demonstrate that the distinct writing preference at the word-level plays a key role in MGT detection. Therefore, we conduct two complementary validations<sup>3</sup>: *i) in the frequency domain*, we examine whether high-frequency components are particularly sensitive to token-level changes; and *ii) in the feature space*, we assess whether low-frequency components effectively capture global structural features. These findings support the subsequent use of low-frequency filtering and frequency-domain alignment to improve DG in MGT detection.

**Analyzing the Correlation Between Frequency Components and Feature Space.** To validate whether different frequency components effectively capture distinct linguistic features, we apply three types of content-preserving perturbations in the

<sup>3</sup>Our experimental data are identical to those used in Figure 1.

feature space, namely token perturbations (word-level), sentence reordering (sentence-level), and theme transformations (document-level). As shown in Table 1, in the feature space, token-level perturbations tend to cause larger MAE<sup>4</sup> values in the high-frequency components, while theme transformations primarily increase the MAE in the low-frequency components compared to other perturbations. This indicates that high-frequency components are more sensitive to token-level changes and predominantly encode token-level features. Conversely, low-frequency components are more sensitive to document-level perturbations, capturing domain-specific information (e.g., topic, style). Further analysis of domain shift is provided in Appendix B.3.

Perturbation	low-frequency	mid-	high-
Theme-Transformation	<b>0.0072</b>	0.0166	0.0349
Sentence-Reordering	0.0002	<b>0.0744</b>	0.0250
Token-Replacement	0.0041	0.0867	<b>0.3225</b>
Token-Delete	0.0034	0.2453	<b>0.4122</b>
Token-Repetition	0.0048	0.2703	<b>0.5592</b>

Table 1: MAE Shift in Frequency Bands.

**Topic Coherence in Feature Space.** To evaluate the coherence between frequency components and global semantic features, we project each frequency band back into the feature space via IDFT and compute its similarity to the original document-level embedding using BERTScore<sup>5</sup>. As shown in Table 2, low-frequency components exhibit the highest similarity, whereas high-frequency components score the lowest, indicating that low-frequency features better preserve global topical information.

Perturbation	low-frequency	mid-	high-
BERTSore	<b>0.8671</b>	0.4062	0.1945

Table 2: Topic Coherence Compared to the Original Text.

<sup>4</sup>Mean Absolute Error is a standard metric for measuring signal-level differences, and a higher MAE reflects greater spectral deviation between the perturbed and original inputs in the frequency domain (Yi et al., 2023). The perturbation rate is 15%.

<sup>5</sup>BERTScore (Angelov and Inkpen, 2024) is a widely used metric for assessing the topic coherence of learned representations. Higher scores indicate stronger global semantic coherence between the reconstructed embeddings and the original embeddings.

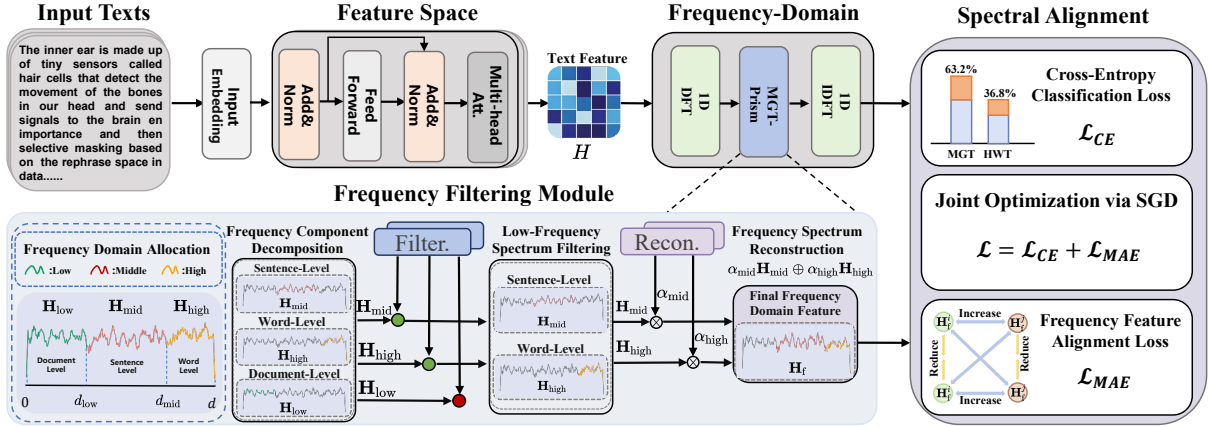


Figure 2: Overview of MGT-Prism. In the Low Frequency Filtering Module (Sec. 4.1), we transform features from feature space into the frequency domain, where we analyze information distribution across multiple frequency bands (*i.e.*, low-, mid-, and high-frequency). Then, we propose a low-frequency filtering module to suppress redundant features shared between MGT and HWT. In the Spectral Alignment stage (Sec. 4.2), we compute the global frequency spectrum distribution and reconstruct the frequency components accordingly. Furthermore, we design a frequency alignment loss to enhance DG.

## 4 Methodology

The workflow of the proposed MGT-Prism is shown in Fig. 2, comprising two main components: a Low Frequency Filtering Module (LFF), and a Spectrum Alignment Module (SAM), to reduce the domain gap for intra-class samples. LFF cuts out the low-frequency band to reduce domain-sensitive but task-irrelevant features. SAM sets an optimization objective to mitigate domain gap for data within the same class. The learning process of our algorithm is described in Appendix A.3.

### 4.1 Low Frequency Filtering Module

Previous studies (Tamkin et al., 2020b; Sun et al., 2024) on frequency domain analysis in the field of natural language processing and analysis about the discrepancy between MGT and HWT (Chen et al., 2025; Liu et al., 2024b) observe that the low-frequency band corresponds with document-level features. We transform the text input into a frequency domain representation (Lee-Thorp et al., 2021; Yi et al., 2023) and decompose it into three frequency bands (*i.e.*, low, mid, and high), and propose a low-frequency filtering module to suppress the common features between MGT and HWT.

With the improvement of text generation capabilities of LLMs, MGT hardly differs from HWT at the discourse level (Chen et al., 2025; Liu et al., 2024a). In frequency domain analysis, this phenomenon is reflected in the fact that low frequency components are often smoother (Tamkin et al., 2020a). Furthermore, in the DG settings, changes

in style, generator, or theme are more likely to cause the migration of text document-level features. Therefore, we filter out low-frequency components  $\mathbf{H}_{\text{low}}$  while retaining mid and high frequency components to enhance the classifier’s ability to distinguish between MGT and HWT under DG. The final frequency domain features after low-frequency filtering can be expressed as:

$$d_{\text{mid}} = \left\lceil \frac{N}{s_{\text{num}}} \cdot \tau + (N - d_{\text{low}}) \cdot (1 - \tau) \right\rceil, \quad (8)$$

$$\mathbf{H}_{\text{mid}} = \{\mathbf{h}_k\}_{k=d_{\text{low}}+1}^{d_{\text{mid}}}, \quad \mathbf{H}_f = \mathbf{H}_{\text{mid}} \oplus \mathbf{H}_{\text{high}}, \quad (9)$$

where  $\tau \in [0, 1]$  is the scaling factor. By adjusting  $\tau$ , the mid-frequency band will be affected by the number of sentences and the remaining frequency bands, avoiding the overflow problem caused by too few or too many sentences.  $\oplus$  denote the concatenation operation. From the perspective of natural text,  $\mathbf{H}_f$  retains more fine-grained information of words and sentences in the text input  $x$ .

### 4.2 Spectral Alignment Module

**Frequency Spectrum Reconstruction.** After removing the low-frequency features that are easily affected by domain-shift, we restore the remaining frequency-domain features to the original features to reduce the detector’s excessive attention to specific domain information during the training process. Specifically, given a batch of training data  $D = \{x_b, y_b\}_{b=0}^{B-1}$  with  $B$  text-label

pairs. Through the previous section, we can obtain the frequency domain features representation  $\{\mathbf{H}_f^b\}_{b=0}^{B-1} = \{\mathbf{H}_{\text{mid}}^b \oplus \mathbf{H}_{\text{high}}^b\}_{b=0}^{B-1}$  of each input text  $T_b$ . Subsequently, we compute the average modulus values of the frequency-domain features within the mid- and high-frequency intervals for the current batch  $D$ . These values are then compared with the corresponding average modulus values of the entire training dataset to determine the weighting factors  $\alpha_{\text{mid}}$  and  $\alpha_{\text{high}}$  for reconstructing the features in the mid and high frequency bands.

$$\mu_{\text{mid}} = \frac{1}{B} \sum_{b=0}^{B-1} \left| \mathbf{H}_{\text{mid}}^b \right|, \quad \mu_{\text{high}} = \frac{1}{B} \sum_{n=0}^{B-1} \left| \mathbf{H}_{\text{high}}^b \right|, \quad (10)$$

$$\alpha_{\text{mid}} = \frac{\bar{\mu}_{\text{mid}}}{\mu_{\text{mid}}}, \quad \alpha_{\text{high}} = \frac{\bar{\mu}_{\text{high}}}{\mu_{\text{high}}}, \quad (11)$$

where  $|\cdot|$  represents the modulus operation,  $\bar{\mu}_{\text{mid}}$  and  $\bar{\mu}_{\text{high}}$  represent the average modulus values of the mid and high frequency of the entire training set, respectively. Therefore, the final frequency domain features can be expressed as:

$$\mathbf{H}_f^b = \alpha_{\text{mid}} \mathbf{H}_{\text{mid}}^b \oplus \alpha_{\text{high}} \mathbf{H}_{\text{high}}^b, \quad 0 \leq b \leq (B-1). \quad (12)$$

The natural text features after filtering and reconstruction can be expressed as:

$$H_f^b = \text{IDFT}(\mathbf{H}_f^b), \quad 0 \leq b \leq (B-1), \quad (13)$$

By low frequency filtering and reconstructing frequency domain features, we strip away the global information that is less discriminative between MGT and HWT, thereby promoting more effective learning of local features.

**Frequency Spectrum Alignment.** To further promote feature alignment among samples from the same class and enhance generalization to unseen domains, we introduce a frequency domain feature alignment loss  $\mathcal{L}_{\text{MAE}}$ . Building on the standard signal level dissimilarity metric, mean absolute error (MAE) (Yi et al., 2023),  $\mathcal{L}_{\text{MAE}}$  reduces distributional differences by minimizing the average  $L_1$  distance (Zhou et al., 2021) between samples from the same class in the frequency domain.

Specifically, given a batch of training data  $D$  and corresponding frequency features  $\{\mathbf{H}_f^b\}_{b=0}^{B-1}$ , for any frequency features  $\mathbf{H}_f^b$ , let the set of remaining frequency features with the same label as  $D_{\text{pos}}$ , and the set of remaining frequency features with different labels be denoted as  $D_{\text{neg}}$ . Then the loss function  $\mathcal{L}_{\text{MAE}}$  can be defined as:

$$\mathcal{L}_{\text{pos}} = \mathbb{E}_{\mathbf{H}_f^b \in D} \mathbb{E}_{\mathbf{H}_f^i \in D_{\text{pos}}} (\|(|\mathbf{H}_f^b| - |\mathbf{H}_f^i|)\|_1), \quad (14)$$

$$\mathcal{L}_{\text{neg}} = \mathbb{E}_{\mathbf{H}_f^b \in D} \mathbb{E}_{\mathbf{H}_f^i \in D_{\text{neg}}} (\max(0, (\xi - \|(|\mathbf{H}_f^b| - |\mathbf{H}_f^i|)\|_1))), \quad (15)$$

$$\mathcal{L}_{\text{MAE}} = \mathcal{L}_{\text{pos}} + \mathcal{L}_{\text{neg}}, \quad (16)$$

where  $\|\cdot\|_1$  denotes the MAE computed over the modulus values,  $\xi$  represents the maximum same class distance, which is used to control the distance between samples with different labels. Then, the total loss is computed by:

$$\mathcal{L} = \mathcal{L}_{\text{CE}} + \mathcal{L}_{\text{MAE}}, \quad (17)$$

where the cross-entropy classification loss  $\mathcal{L}_{\text{CE}}$  is computed on natural text features  $H_f^b$ , describing in Eq. (13), and corresponding labels  $Y_b$ .

## 5 Experiments

### 5.1 Experiment Settings

To evaluate DG in MGT detection, we conduct extensive experiments on three open-source datasets, including M4 (Wang et al., 2023c), DetectRL (Wu et al., 2024), and MAGE (Li et al., 2024) dataset, under three experimental settings: *i*) **Cross-Domain**, composed of the DetectRL and MAGE datasets, and including MGTs from Opinion Statement (Opinion.S), Question Answering (Question.A), Story generation (Story.G), and Scientific Writing (Scientific.W). *ii*) **Cross-Generator**, composed of the M4 and MAGE datasets, in which we obtain MGTs generated by Flan-T5 (Chung et al., 2024), ChatGPT (OpenAI, 2022), GLM (Zeng et al., 2022), and LLaMA (Touvron et al., 2023). *iii*) **Cross-Scale**, based on the MAGE dataset, including MGTs generated by LLaMA2-13B, LLaMA2-30B, and LLaMA2-65B.

We randomly select 1000 samples from the original training set, balanced across datasets, domains, and categories. Training is performed for 30 epochs using AdamW ( $\epsilon = 2 \times 10^{-5}$ ), with a learning rate of 0.01 and a scaling factor  $\tau$  of 0.6. More details are shown in the Appendix A.

### 5.2 Competitors

We evaluate MGT-Prism against nine methods for MGT detection, including metric-based and fine-tuned detectors.

**Metric-based detectors.** Log-probabilities from a generative LM are often used for classification with a predefined threshold <sup>6</sup>, including *GLTR*

<sup>6</sup>We utilizing the GPT-Neo-2.7B (Black et al., 2021) to align with Fast-DetectGPT (Bao et al., 2024) experiments.

Method			Metric-based				Model-based					
Dataset	Test data	Metric	GLTR	DetectGPT	Fast-Dete.	Binoculars	RoBERTa <sup>†</sup>	RADAR	Ghostbuster	PECOLA <sup>†</sup>	ImBD	MGT-Prism <sup>†</sup>
Cross-Generator	FLAN-T5	Acc	67.10	60.30	74.70	63.46	86.80 <sub>1.90</sub>	65.82 <sub>4.06</sub>	79.55 <sub>4.16</sub>	86.30 <sub>1.80</sub>	71.55 <sub>2.06</sub>	<b>89.62</b> <sub>1.67</sub>
		F1	52.11	49.33	60.70	52.70	85.95 <sub>1.76</sub>	60.75 <sub>5.06</sub>	75.45 <sub>4.26</sub>	86.20 <sub>1.62</sub>	65.54 <sub>3.46</sub>	<b>89.02</b> <sub>1.97</sub>
	ChatGPT	Acc	78.12	60.71	76.60	<b>87.60</b>	85.01 <sub>3.74</sub>	61.50 <sub>3.01</sub>	77.06 <sub>2.04</sub>	84.21 <sub>3.50</sub>	85.68 <sub>3.76</sub>	<b>88.96</b> <sub>2.03</sub>
		F1	62.01	68.70	69.70	<b>87.63</b>	84.65 <sub>1.76</sub>	69.95 <sub>5.15</sub>	72.65 <sub>5.07</sub>	84.25 <sub>2.01</sub>	79.55 <sub>3.26</sub>	<b>89.22</b> <sub>1.67</sub>
	GLM	Acc	75.50	73.20	76.02	<b>95.28</b>	89.94 <sub>1.68</sub>	70.04 <sub>4.09</sub>	80.94 <sub>2.58</sub>	89.60 <sub>2.70</sub>	87.48 <sub>2.06</sub>	<b>92.42</b> <sub>1.56</sub>
		F1	60.10	62.43	69.62	<b>95.36</b>	86.95 <sub>2.06</sub>	62.90 <sub>3.09</sub>	74.65 <sub>4.13</sub>	84.22 <sub>2.01</sub>	89.04 <sub>3.76</sub>	<b>92.82</b> <sub>1.67</sub>
	LLaMA	Acc	72.40	70.80	79.65	80.95	85.31 <sub>2.67</sub>	70.12 <sub>4.67</sub>	80.45 <sub>2.76</sub>	82.99 <sub>2.61</sub>	84.22 <sub>3.07</sub>	<b>87.61</b> <sub>1.74</sub>
		F1	60.17	62.33	61.60	83.15	80.85 <sub>3.66</sub>	67.95 <sub>3.05</sub>	79.65 <sub>4.01</sub>	84.20 <sub>1.92</sub>	85.34 <sub>2.06</sub>	<b>87.20</b> <sub>1.77</sub>
Cross-Domain	Opinion.S	Acc	71.15	70.40	76.30	<b>95.04</b>	93.61 <sub>2.65</sub>	74.39 <sub>3.05</sub>	90.97 <sub>2.91</sub>	93.49 <sub>3.06</sub>	94.85 <sub>0.33</sub>	<b>96.06</b> <sub>1.08</sub>
		F1	65.60	60.70	72.70	<b>95.20</b>	92.24 <sub>1.93</sub>	60.04 <sub>2.56</sub>	91.27 <sub>1.83</sub>	91.14 <sub>2.20</sub>	92.58 <sub>2.06</sub>	<b>96.90</b> <sub>1.53</sub>
	Question.A	Acc	72.90	72.20	76.90	93.60	93.92 <sub>1.15</sub>	72.52 <sub>1.95</sub>	92.82 <sub>4.06</sub>	94.12 <sub>2.95</sub>	93.23 <sub>0.92</sub>	<b>96.53</b> <sub>1.45</sub>
		F1	70.60	76.10	70.80	<b>93.62</b>	93.04 <sub>1.93</sub>	78.64 <sub>3.64</sub>	91.45 <sub>2.74</sub>	92.64 <sub>2.10</sub>	92.28 <sub>1.06</sub>	<b>96.20</b> <sub>1.13</sub>
	Scientific.W	Acc	41.24	50.90	66.90	<b>79.92</b>	70.43 <sub>8.29</sub>	70.18 <sub>10.79</sub>	62.73 <sub>9.19</sub>	68.90 <sub>9.17</sub>	<b>80.26</b> <sub>5.10</sub>	79.88 <sub>7.22</sub>
		F1	32.60	35.22	48.70	<b>79.95</b>	61.94 <sub>8.23</sub>	50.64 <sub>8.94</sub>	55.95 <sub>6.93</sub>	60.25 <sub>7.80</sub>	74.28 <sub>4.56</sub>	77.80 <sub>7.43</sub>
	Story.G	Acc	70.60	60.22	76.70	90.62	98.62 <sub>0.42</sub>	75.76 <sub>3.23</sub>	95.60 <sub>1.32</sub>	98.20 <sub>0.40</sub>	92.75 <sub>0.54</sub>	<b>98.96</b> <sub>0.25</sub>
		F1	65.25	67.06	70.90	90.90	98.04 <sub>1.63</sub>	70.84 <sub>3.06</sub>	94.65 <sub>2.63</sub>	97.09 <sub>2.00</sub>	93.08 <sub>2.76</sub>	<b>98.90</b> <sub>1.03</sub>
Cross-Scale	LLaMa-13b	Acc	73.92	71.20	82.90	94.65	93.85 <sub>1.72</sub>	76.28 <sub>2.60</sub>	90.95 <sub>1.92</sub>	93.48 <sub>2.12</sub>	94.91 <sub>0.95</sub>	<b>95.94</b> <sub>1.62</sub>
		F1	70.60	75.02	78.98	<b>93.70</b>	92.74 <sub>1.50</sub>	70.60 <sub>3.14</sub>	92.50 <sub>1.93</sub>	92.14 <sub>2.01</sub>	92.78 <sub>2.06</sub>	<b>95.91</b> <sub>1.70</sub>
	LLaMa-30b	Acc	77.90	73.20	80.62	93.65	93.28 <sub>1.20</sub>	77.49 <sub>1.25</sub>	94.44 <sub>2.10</sub>	94.44 <sub>1.19</sub>	92.26 <sub>1.71</sub>	<b>94.67</b> <sub>1.20</sub>
		F1	73.90	77.25	84.21	<b>94.02</b>	92.60 <sub>1.93</sub>	71.64 <sub>3.14</sub>	92.15 <sub>2.76</sub>	93.04 <sub>1.40</sub>	90.28 <sub>3.66</sub>	<b>93.70</b> <sub>1.73</sub>
	LLaMa-65b	Acc	75.60	74.90	77.92	92.05	92.24 <sub>1.63</sub>	74.70 <sub>2.60</sub>	91.95 <sub>2.03</sub>	92.06 <sub>1.10</sub>	86.38 <sub>2.90</sub>	<b>93.60</b> <sub>1.13</sub>
		F1	70.70	72.12	78.09	91.40	92.10 <sub>1.43</sub>	70.14 <sub>3.20</sub>	92.05 <sub>2.13</sub>	91.14 <sub>1.70</sub>	83.48 <sub>3.96</sub>	<b>93.92</b> <sub>1.73</sub>
Average	Acc	70.58	67.09	76.83	87.82		<b>89.36</b>	71.70	85.04	88.89	87.59	<b>92.21</b>
	F1	62.14	64.20	69.63	87.06		<b>87.37</b>	66.73	82.94	86.93	85.29	<b>91.96</b>

Table 3: Accuracy and F1 score (%) of MGT-Prism and baseline methods for MGT detection under the DG setting. The results are average values of 10 runs with different random seeds. The subscript means the standard deviation (e.g., 93.92<sub>1.73</sub> means  $93.92 \pm 1.73$ ). Metric-based methods’ results are deterministic, so we do not report standard deviation. Also, these metric-based methods must have the white-box generator as the base model, which is different from the model-based methods. <sup>†</sup> denotes using the RoBERTa-base (125M) as the backbone model. The best and second-best are **bolded** and underlined respectively.

(Gehrmann et al., 2019), DetectGPT (Mitchell et al., 2023), Fast-DetectGPT (Bao et al., 2024), Binoculars (Hans et al., 2024)<sup>7</sup>.

**Fine-tuned detectors.** Supervised detectors trained on a PLM, typically optimized with a classification loss, including RoBERTa (Liu et al., 2019), Ghostbuster (Verma et al., 2023), RADAR (Hu et al., 2023), PECOLA (Liu et al., 2024a), ImBD (Chen et al., 2025).

### 5.3 Performance Comparison

We report the experimental results in Table 3. We first compare MGT-Prism with state-of-the-art metric-based and model-based detectors. In the DG setting, compared to the strongest baselines RoBERTa and Binoculars, MGT-Prism achieves average improvements of 3.62% in accuracy and 4.75% in F1 score, demonstrating strong DG. Broadly speaking, the mostly fine-tuned detectors outperform metric-based methods across all datasets because the performance significantly drops when the scoring model differs from the target model (Mitchell et al., 2023). Moreover, the detection results in the cross-generator setting

are generally lower than those in the cross-domain and cross-scale settings, likely due to more severe domain shifts introduced by different generators. It demonstrates that the different generation paradigms across models lead to a larger domain shift, degrading the model performance. In the cross-domain setting, testing the model on the Scientific.W dataset leads to consistent low accuracy below 81% because of the large difference between general writing and the scitific writing which uses more technical words (Liu et al., 2024a).

### 5.4 Ablation Study

We conduct ablation experiments to understand the contribution of each component of MGT-Prism in the cross-generator setting. The core components we examine are: Low Frequency Filtering Module (LFF), Frequency Spectrum Reconstruction (FSR), and Frequency Spectrum Alignment (FSA). As shown in Table 4, we find that every block in MGT-Prism contributes to the DG of MGT detector, shown by the improvement over the RoBERTa baseline. Moreover, the FSA module contributes to the detection performance most, indicating the alignment of frequency-domain features plays an important role in mitigating domain shift. In average, the combination of two components is always

<sup>7</sup>Under the original Falcon-7B and Falcon-7B-Instruct setting.

Modules			Cross-Generator				
LFF	FSR	FSA	Flan-T5	ChatGPT	GLM	LLaMa	Avg.
-	-	-	85.95	84.65	86.95	80.85	84.60
✓	-	-	87.84	85.61	88.61	84.92	86.75
-	✓	-	86.40	84.82	89.15	83.91	86.07
-	-	✓	88.05	85.27	89.01	85.28	86.90
✓	✓	-	87.42	86.49	90.02	85.81	87.44
✓	-	✓	88.04	88.05	89.99	85.71	87.94
-	✓	✓	87.21	86.85	89.25	86.93	87.56
✓	✓	✓	<b>89.02</b>	<b>89.23</b>	<b>92.82</b>	<b>87.20</b>	<b>89.57</b>

Table 4: **F1 score (%) for Ablation study on different module combinations.** ✓ means that we keep the corresponding block and - means the block is removed.

superior to only incorporating one module into the training process, indicating that different modules are complementary to each other and collectively boost the DG of MGT detector. We also discuss the effects of different scale factors and test lengths in Appendix B.1 and B.2.

## 5.5 Discussion

**Effect of Individual Frequency Components.** Compared to style and theme, which are coarse-grained and unstable across domains or generators, sentence structure and token-level statistics provide more reliable signals for detection. While many existing methods exploit such fine-grained cues (e.g., LM probabilities and perturbations), our approach further aligns multi-granular features with frequency bands. As shown in Table 5, results reveal that using only the low-frequency band leads to an average F1 score of 83.22%, representing a 1.38% drop compared to the all-features model. In contrast, isolating the mid- and high-frequency bands individually leads to performance gains of 1.01% and 1.47%, respectively, compared to the all-features model.

Modules			Cross-Generator				
Low-	Mid-	High-	Flan-T5	ChatGPT	GLM	LLaMa	Avg.
✓	-	-	85.01	83.64	85.29	79.96	83.22
-	✓	-	86.01	<b>85.31</b>	88.64	<b>83.49</b>	85.61
-	-	✓	<b>87.65</b>	85.07	<b>89.49</b>	83.08	<b>86.07</b>
✓	✓	✓	85.95	84.65	86.95	80.85	84.60

Table 5: F1 score from Ablation on Individual Components.

**Robustness under Perturbation.** We test the robustness of detectors under four attacks (*i.e.*, Delete, Insert, Repeat, and Generate) with a perturbation rate of 15%, following Wang et al. (2024). As shown in Table 6, our method exhibits a consis-

tently smaller drop in F1 score than the baselines RoBERTa and Binoculars. MGT-Prism achieves an average improvement of 5.29% in F1 score. Specifically, under the deletion and repetition perturbations, the averaged F1 score of MGT-Prism decreases by only 5.10% and 5.23% in the two scenarios (*i.e.*, cross-generator and cross-domain), underscoring its remarkable robustness. The complete evaluation results for all attacks are provided in the Appendix C.1.

Perturbation	Delete	Insert	Repeat	Generate	Avg.
<i>Binoculars</i>					
Cross-Generator	65.41	65.12	65.66	59.59	63.95
Cross-Domain	83.97	81.10	82.45	67.45	78.74
Cross-Scale	84.78	76.19	68.53	61.55	72.76
<i>RoBERTa-base</i>					
Cross-Generator	75.065	59.91	81.285	60.03	69.07
Cross-Domain	85.35	74.81	81.40	72.90	78.61
Cross-Scale	83.15	73.22	68.16	65.06	72.39
<i>MGT-Prism</i>					
Cross-Generator	79.61	67.99	84.58	67.40	74.90
Cross-Domain	89.32	77.12	85.12	77.67	82.30
Cross-Scale	85.74	76.53	73.95	69.51	76.43

Table 6: **Performance on diverse perturbation attacks.** Results are reported as the average F1 score (%) across three generalization settings and four perturbation scenarios. GPT-2 XL (1.5B) (Solaiman et al., 2019) is employed to construct perturbations, including generating and inserting.

**Applicability to Different Backbones.** We evaluate the effectiveness of MGT-Prism with RoBERTa-large and BERT-large and Qwen3-0.6B (Zhang et al., 2025) as the backbones in both in-domain (IND) and DG settings. As shown in Table 7, MGT-Prism always outperforms vanilla fine-tuning with different backbones, in all settings. Specifically, MGT-Prism improves over the vanilla fine-tuning by 1.16% and 2.11% in RoBERTa-large, and by an average of 1.53% on Qwen3-0.6B. The results demonstrate that MGT-Prism is applicable to different backbones with different scales. More test results are shown in Appendix C.2. We also visualization of feature distribution in Appendix C.3.

**Visualization of Feature Distribution.** To better understand the improved generalization performance of our method in detecting MGT under domain shifts, we extract features of the test samples from the final hidden layer of both RoBERTa-base and MGT-Prism, and use t-SNE (Van der Maaten and Hinton, 2008) to project them into a 2D space for visualization, as illustrated in Fig. 3. Under

In-domain (IND)						
Model	Method	Generator	Domain	Scale	Avg.	
RoBERTa-base	base	93.45	96.01	94.90	94.78	
	MGT-Prism	94.89	97.43	95.32	95.88	
RoBERTa-large	base	94.75	97.87	96.24	96.28	
	MGT-Prism	<b>96.05</b>	<b>98.98</b>	<b>97.29</b>	<b>97.44</b>	
BERT-large	base	88.21	94.49	92.23	91.64	
	MGT-Prism	90.01	95.24	92.94	92.73	
QWen3-0.6B	base	93.81	96.82	95.82	95.48	
	MGT-Prism	<u>95.28</u>	<u>98.24</u>	<u>96.49</u>	<u>96.67</u>	
Domain Generalization (DG)						
Model	Method	Generator	Domain	Scale	Avg.	
RoBERTa-large	base	88.13	<u>93.10</u>	93.81	91.49	
	MGT-Prism	<b>90.84</b>	<b>95.02</b>	<b>95.37</b>	<b>93.60</b>	
BERT-large	base	81.4	82.68	89.88	84.17	
	MGT-Prism	84.18	88.71	92.97	88.22	
QWen3-0.6B	base	86.17	89.08	93.86	89.32	
	MGT-Prism	87.47	92.04	<u>95.03</u>	91.19	

Table 7: **F1 score (%) Comparison with Different Backbones.** For the DG setting, the reported results are averaged across all test subsets. For the IND setting, all subcategories are merged for training and testing.

the DG setting, we use the ChatGPT subset as test data and observe that MGT-Prism produces representations with clearer separation between HWT and MGT instances than RoBERTa-base. Moreover, data points with the same label are more tightly clustered. More visualizations across different datasets are reported in Appendix C.3.

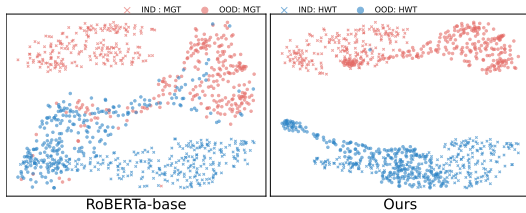


Figure 3: t-SNE Visualization of the Learned [CLS] Embeddings. Comparison between RoBERTa-base and MGT-Prism on IND and DG test sets.

## 6 Conclusion

In this work, we focus on enhancing the domain generalization ability of MGT detectors with concentration on mitigating domain shift brought by data sources. We transfer the text representation to frequency domain using DFT and find that the spectra of text features mitigate the domain shift among intra-class samples. Based on the decomposability of frequency domain, we design a low-frequency spectrum filtering module to remove the low-frequency feature which is more affected by the domain shift. Moreover, we align the spectra of intra-class samples from different domains with

frequency spectrum alignment module to mitigate the domain shift, therefore enabling the model to learn task-specific and domain-invariant features from frequency domain. Experimental results show that our method outperforms SOTA metric-based and model-based baselines. We hope that our work can inspire future research in AI-generated content detection in other modalities, and serve as a foundation for developing a unified detecting approach.

## Ethics Statement

MGT-Prism is designed to assist users in reasonably and accurately identifying MGT. Our goal is to develop a generalizable method that can be extended to other modalities, such as image and audio, and to inspire progress toward more robust MGT detectors. While we aim to support the responsible development and deployment of detection techniques, we explicitly discourage any malicious use of our work, particularly attempts to evade or undermine detection systems. All datasets used in this study are publicly available.

## References

Ebtessam Almazrouei, Hamza Alobeidli, Abdulaziz Alshamsi, Alessandro Cappelli, Ruxandra Cojocaru, Merouane Debbah, Etienne Goffinet, Daniel Heslow, Julien Launay, Quentin Malartic, et al. 2023. Falcon-40b: an open large language model with state-of-the-art performance.

Dimo Angelov and Diana Inkpen. 2024. Topic modeling: Contextual token embeddings are all you need. In *Findings of the Association for Computational Linguistics: EMNLP 2024*, pages 13528–13539.

Guangsheng Bao, Yanbin Zhao, Zhiyang Teng, Linyi Yang, and Yue Zhang. 2023. Fast-detectgpt: Efficient zero-shot detection of machine-generated text via conditional probability curvature. In *The Twelfth International Conference on Learning Representations*.

Guangsheng Bao, Yanbin Zhao, Zhiyang Teng, Linyi Yang, and Yue Zhang. 2024. **Fast-detectGPT: Efficient zero-shot detection of machine-generated text via conditional probability curvature**. In *The Twelfth International Conference on Learning Representations*.

Sid Black, Gao Leo, Phil Wang, Connor Leahy, and Stella Biderman. 2021. GPT-Neo: Large Scale Autoregressive Language Modeling with Mesh Tensorflow.

Ronald N. Bracewell. 1986. *The Fourier Transform and Its Applications*, 2nd edition. McGraw-Hill.

Defu Cao, Yujing Wang, Juanyong Duan, Ce Zhang, Xia Zhu, Congrui Huang, Yunhai Tong, Bixiong Xu, Jing Bai, Jie Tong, et al. 2020. Spectral temporal graph neural network for multivariate time-series forecasting. *Advances in neural information processing systems*, 33:17766–17778.

Jiaqi Chen, Xiaoye Zhu, Tianyang Liu, Ying Chen, Chen Xinhui, Yiwen Yuan, Chak Tou Leong, Zuchao Li, Long Tang, Lei Zhang, et al. 2025. Imitate before detect: Aligning machine stylistic preference for machine-revised text detection. In *Proceedings of the AAAI Conference on Artificial Intelligence*, volume 39, pages 23559–23567.

Krzysztof Choromanski, Valerii Likhoshesterov, David Dohan, Xingyou Song, Andreea Gane, Tamas Sarlos, Peter Hawkins, Jared Davis, David Belanger, Lucy Colwell, et al. 2020. Masked language modeling for proteins via linearly scalable long-context transformers. *arXiv preprint arXiv:2006.03555*.

Hyung Won Chung, Le Hou, Shayne Longpre, Barret Zoph, Yi Tay, William Fedus, Yunxuan Li, Xuezhi Wang, Mostafa Dehghani, Siddhartha Brahma, et al. 2024. Scaling instruction-finetuned language models. *Journal of Machine Learning Research*, 25(70):1–53.

Wei Fan, Shun Zheng, Xiaohan Yi, Wei Cao, Yanjie Fu, Jiang Bian, and Tie-Yan Liu. 2022. Depts: Deep expansion learning for periodic time series forecasting. *arXiv preprint arXiv:2203.07681*.

Ronglong Fang and Yuesheng Xu. 2024. **Addressing spectral bias of deep neural networks by multi-grade deep learning**. In *Advances in Neural Information Processing Systems*, volume 37, pages 114122–114146. Curran Associates, Inc.

Jun Gao, Changlong Yu, Wei Wang, Huan Zhao, and Ruiyong Xu. 2022. Mask-then-fill: A flexible and effective data augmentation framework for event extraction. In *Conference on Empirical Methods in Natural Language Processing*.

Sebastian Gehrmann, Hendrik Strobelt, and Alexander M Rush. 2019. Gltr: Statistical detection and visualization of generated text. In *Proceedings of the 57th Annual Meeting of the Association for Computational Linguistics: System Demonstrations*, pages 111–116.

Beliz Gunel, Jingfei Du, Alexis Conneau, and Ves Stoyanov. 2021. Supervised contrastive learning for pre-trained language model fine-tuning. In *International Conference on Learning Representations*.

Jintao Guo, Na Wang, Lei Qi, and Yinghuan Shi. 2023. **Aloft: A lightweight mlp-like architecture with dynamic low-frequency transform for domain generalization**. In *Proceedings of the IEEE/CVF conference on computer vision and pattern recognition*, pages 24132–24141.

Abhimanyu Hans, Avi Schwarzschild, Valeria Cherepanova, Hamid Kazemi, Aniruddha Saha, Micah Goldblum, Jonas Geiping, and Tom Goldstein. 2024. Spotting llms with binoculars: Zero-shot detection of machine-generated text. *arXiv preprint arXiv:2401.12070*.

Xiaomeng Hu, Pin-Yu Chen, and Tsung-Yi Ho. 2023. **Radar: Robust ai-text detection via adversarial learning**. *arXiv preprint arXiv:2307.03838*.

Salman H Khan, Munawar Hayat, and Fatih Porikli. 2019. Regularization of deep neural networks with spectral dropout. *Neural Networks*, 110:82–90.

Sandeep Kumar, Samarth Garg, Sagnik Sengupta, Tirthankar Ghosal, and Asif Ekbal. 2025. **MixRevDetect: Towards detecting AI-generated content in hybrid peer reviews**. In *Proceedings of the 2025 Conference of the Nations of the Americas Chapter of the Association for Computational Linguistics: Human Language Technologies (Volume 2: Short Papers)*, pages 944–953, Albuquerque, New Mexico. Association for Computational Linguistics.

Laida Kushnareva, Daniil Cherniavskii, Vladislav Mikhailov, Ekaterina Artemova, Serguei Barannikov, Alexander Bernstein, Irina Piontkovskaya, Dmitri Piontkovski, and Evgeny Burnaev. 2021. **Artificial**

text detection via examining the topology of attention maps. In *Proceedings of the 2021 Conference on Empirical Methods in Natural Language Processing*, pages 635–649.

James Lee-Thorp, Joshua Ainslie, Ilya Eckstein, and Santiago Ontanon. 2021. Fnet: Mixing tokens with fourier transforms. *arXiv preprint arXiv:2105.03824*.

Ran Li, Wei Hao, Weiliang Zhao, Junfeng Yang, and Chengzhi Mao. 2025a. Learning to rewrite: Generalized llm-generated text detection.

Yafu Li, Qintong Li, Leyang Cui, Wei Bi, Zhilin Wang, Longyue Wang, Linyi Yang, Shuming Shi, and Yue Zhang. 2024. **MAGE: Machine-generated text detection in the wild**. In *Proceedings of the 62nd Annual Meeting of the Association for Computational Linguistics (Volume 1: Long Papers)*, pages 36–53, Bangkok, Thailand. Association for Computational Linguistics.

Yuanfan Li, Zhaohan Zhang, Chengzhengxu Li, Chao Shen, and Xiaoming Liu. 2025b. Iron sharpens iron: Defending against attacks in machine-generated text detection with adversarial training.

Shengchao Liu, Xiaoming Liu, Yichen Wang, Zehua Cheng, Chengzhengxu Li, Zhaohan Zhang, Yu Lan, and Chao Shen. 2024a. Does detectgpt fully utilize perturbation? bridging selective perturbation to fine-tuned contrastive learning detector would be better. *arXiv preprint arXiv:2402.00263*.

Shengchao Liu, Xiaoming Liu, Yichen Wang, Zehua Cheng, Chengzhengxu Li, Zhaohan Zhang, Yu Lan, and Chao Shen. 2024b. Does DetectGPT fully utilize perturbation? bridging selective perturbation to fine-tuned contrastive learning detector would be better. In *Proceedings of the 62nd Annual Meeting of the Association for Computational Linguistics (Volume 1: Long Papers)*, pages 1874–1889, Bangkok, Thailand. Association for Computational Linguistics.

Xiaoming Liu, Zhaohan Zhang, Yichen Wang, Hang Pu, Yu Lan, and Chao Shen. 2023. Coco: Coherence-enhanced machine-generated text detection under low resource with contrastive learning. In *Proceedings of the 2023 Conference on Empirical Methods in Natural Language Processing*, pages 16167–16188.

Yinhan Liu, Myle Ott, Naman Goyal, Jingfei Du, Mandar Joshi, Danqi Chen, Omer Levy, Mike Lewis, Luke Zettlemoyer, and Veselin Stoyanov. 2019. Roberta: A robustly optimized bert pretraining approach. *arXiv preprint arXiv:1907.11692*.

Eric Mitchell, Yoonho Lee, Alexander Khazatsky, Christopher D. Manning, and Chelsea Finn. 2023. Detectgpt: Zero-shot machine-generated text detection using probability curvature. *ICML 2023*.

OpenAI. 2022. Chatgpt. Website.

Shushanta Pudasaini, Luis Miralles, David Lillis, and Marisa Llorens Salvador. 2025. Benchmarking AI text detection: Assessing detectors against new datasets, evasion tactics, and enhanced LLMs. In *Proceedings of the 1st Workshop on GenAI Content Detection (GenAIDetect)*, pages 68–77, Abu Dhabi, UAE. International Conference on Computational Linguistics.

Oren Rippel, Jasper Snoek, and Ryan P Adams. 2015. Spectral representations for convolutional neural networks. *Advances in neural information processing systems*, 28.

Yuhui Shi, Qiang Sheng, Juan Cao, Hao Mi, Beizhe Hu, and Danding Wang. 2024. Ten words only still help: Improving black-box ai-generated text detection via proxy-guided efficient re-sampling. In *Proceedings of the Thirty-Third International Joint Conference on Artificial Intelligence, IJCAI-2024*, page 494–502. International Joint Conferences on Artificial Intelligence Organization.

KaShun Shum, Shizhe Diao, and Tong Zhang. 2023. Automatic prompt augmentation and selection with chain-of-thought from labeled data. *arXiv preprint arXiv:2302.12822*.

Irene Solaiman, Miles Brundage, Jack Clark, Amanda Askell, Ariel Herbert-Voss, Jeff Wu, Alec Radford, Gretchen Krueger, Jong Wook Kim, Sarah Krep, et al. 2019. Release strategies and the social impacts of language models. *arXiv preprint arXiv:1908.09203*.

Peng Sun, Yao Zhu, Yunjian Zhang, Xiu Yan, Zizhe Wang, and Xiangyang Ji. 2024. Unleashing the potential of large language models through spectral modulation. In *Findings of the Association for Computational Linguistics: EMNLP 2024*, pages 3892–3911, Miami, Florida, USA. Association for Computational Linguistics.

Jihoon Tack, Sangwoo Mo, Jongheon Jeong, and Jinwoo Shin. 2020. Csi: Novelty detection via contrastive learning on distributionally shifted instances. *Advances in neural information processing systems*, 33:11839–11852.

Alex Tamkin, Dan Jurafsky, and Noah Goodman. 2020a. Language through a prism: A spectral approach for multiscale language representations. *Advances in Neural Information Processing Systems*, 33:5492–5504.

Alex Tamkin, Dan Jurafsky, and Noah Goodman. 2020b. Language through a prism: A spectral approach for multiscale language representations.

Hugo Touvron, Thibaut Lavril, Gautier Izacard, Xavier Martinet, Marie-Anne Lachaux, Timothée Lacroix, Baptiste Rozière, Naman Goyal, Eric Hambro, Faisal Azhar, et al. 2023. Llama: Open and efficient foundation language models. *arXiv preprint arXiv:2302.13971*.

Laurens Van der Maaten and Geoffrey Hinton. 2008. Visualizing data using t-sne. *Journal of machine learning research*, 9(11).

Vivek Verma, Eve Fleisig, Nicholas Tomlin, and Dan Klein. 2023. Ghostbuster: Detecting text ghost-written by large language models. *arXiv preprint arXiv:2305.15047*.

Pengyu Wang, Linyang Li, Ke Ren, Botian Jiang, Dong Zhang, and Xipeng Qiu. 2023a. **SeqXGPT: Sentence-level AI-generated text detection**. In *Proceedings of the 2023 Conference on Empirical Methods in Natural Language Processing*, pages 1144–1156, Singapore. Association for Computational Linguistics.

Pengyu Wang, Linyang Li, Ke Ren, Botian Jiang, Dong Zhang, and Xipeng Qiu. 2023b. **SeqXGPT: Sentence-level AI-generated text detection**. In *The 2023 Conference on Empirical Methods in Natural Language Processing*.

Yichen Wang, Shangbin Feng, Abe Hou, Xiao Pu, Chao Shen, Xiaoming Liu, Yulia Tsvetkov, and Tianxing He. 2024. **Stumbling blocks: Stress testing the robustness of machine-generated text detectors under attacks**. In *Proceedings of the 62nd Annual Meeting of the Association for Computational Linguistics (Volume 1: Long Papers)*, pages 2894–2925, Bangkok, Thailand. Association for Computational Linguistics.

Yuxia Wang, Jonibek Mansurov, Petar Ivanov, Jinyan Su, Artem Shelmanov, Akim Tsvigun, Chenxi Whitehouse, Osama Mohammed Afzal, Tarek Mahmoud, Toru Sasaki, et al. 2023c. M4: Multi-generator, multi-domain, and multi-lingual black-box machine-generated text detection. *arXiv preprint arXiv:2305.14902*.

Gerald Woo, Chenghao Liu, Doyen Sahoo, Akshat Kumar, and Steven Hoi. 2022. Cost: Contrastive learning of disentangled seasonal-trend representations for time series forecasting. *arXiv preprint arXiv:2202.01575*.

Haixu Wu, Jiehui Xu, Jianmin Wang, and Mingsheng Long. 2021. Autoformer: Decomposition transformers with auto-correlation for long-term series forecasting. *Advances in neural information processing systems*, 34:22419–22430.

Junchao Wu, Runzhe Zhan, Derek F. Wong, Shu Yang, Xinyi Yang, Yulin Yuan, and Lidia S. Chao. 2024. **Detectrl: Benchmarking llm-generated text detection in real-world scenarios**. In *Advances in Neural Information Processing Systems*, volume 37, pages 100369–100401. Curran Associates, Inc.

Kun Yi, Jingru Fei, Qi Zhang, Hui He, Shufeng Hao, Defu Lian, and Wei Fan. 2024. Filternet: Harnessing frequency filters for time series forecasting. *Advances in Neural Information Processing Systems*, 37:55115–55140.

Kun Yi, Qi Zhang, Wei Fan, Shoujin Wang, Pengyang Wang, Hui He, Ning An, Defu Lian, Longbing Cao, and Zhendong Niu. 2023. Frequency-domain mlps are more effective learners in time series forecasting. *Advances in Neural Information Processing Systems*, 36:76656–76679.

Wenzhen Yue, Yong Liu, Xianghua Ying, Bowei Xing, Ruohao Guo, and Ji Shi. 2025. **Freeformer: Frequency enhanced transformer for multivariate time series forecasting**.

Rowan Zellers, Ari Holtzman, Hannah Rashkin, Yonatan Bisk, Ali Farhadi, Franziska Roesner, and Yejin Choi. 2019. Defending against neural fake news. *Advances in neural information processing systems*, 32.

Aohan Zeng, Xiao Liu, Zhengxiao Du, Zihan Wang, Hanyu Lai, Ming Ding, Zhuoyi Yang, Yifan Xu, Wendi Zheng, Xiao Xia, et al. 2022. Glm-130b: An open bilingual pre-trained model. *arXiv preprint arXiv:2210.02414*.

Yanzhao Zhang, Mingxin Li, Dingkun Long, Xin Zhang, Huan Lin, Baosong Yang, Pengjun Xie, An Yang, Dayiheng Liu, Junyang Lin, Fei Huang, and Jingren Zhou. 2025. Qwen3 embedding: Advancing text embedding and reranking through foundation models. *arXiv preprint arXiv:2506.05176*.

Wenxuan Zhou, Fangyu Liu, and Muha Chen. 2021. Contrastive out-of-distribution detection for pre-trained transformers. In *Proceedings of the 2021 Conference on Empirical Methods in Natural Language Processing*, pages 1100–1111.

## A Implementation Details

This section presents the hyperparameter settings, meta-information, and the learning process of our framework for the DG task in MGT detection. All the experiments are conducted on a single NVIDIA A100 80G GPU.

### A.1 Hyperparameter Details

In this subsection, we provide additional details on hyperparameter settings to support the reproducibility of our method. For each experiment, we randomly select 10 different seeds and report the average test accuracy, as shown in Table 8.

Parameter	Value
Training Epochs	30
Optimizer	AdamW
Learning rate	2e-5
Weight Decay	0.01
Batch Size	32
Pre-trained model	RoBERTa-base
Scaling Factor $\tau$	0.6

Table 8: Implementation details of hyperparameters.

### A.2 Dataset Details

We evaluate MGT-Prism under three generalization settings (*i.e.*, Cross-Generator, Cross-Domain, Cross-Scale) and 11 test sets in total, as shown in Table 9.

### A.3 Learning Process

Our MGT detection framework integrates a Frequency Feature Alignment Loss ( $\mathcal{L}_{MAE}$ ) and a feature space loss ( $\mathcal{L}_{CE}$ ), as detailed in Algorithm 1. It also demonstrates that our method can be extended to a variety of classification tasks to enhance domain generalization.

### A.4 Competitors

We evaluate MGT-Prism against nine methods for MGT detection, including metric-based and fine-tuned detectors.

*GLTR* (Gehrmann et al., 2019), a statistical tool that visualizes token-level prediction probabilities to detect AI-generated content.

*DetectGPT* (Mitchell et al., 2023), a zero-shot metric-based detector that leverages the curvature of the log probability function to differentiate in MGT detection.

*Fast-DetectGPT* (Bao et al., 2024), an optimized version of DetectGPT, it offering significant

---

### Algorithm 1 Learning Process

---

```

1: Input: training dataset  $\mathcal{D}_{train}$ , Valid dataset  $\mathcal{D}_{val}$ , learning rate  $lr$ , Scaling Factor  $\tau$ , Detector model
2: Initialize the pretrained Transformer  $M$ 
3: Compute the global frequency-spectrum distribution over the training set  $\mathcal{D}_{train}$ .
4: for epoch  $e = 1 \dots epoch$  do
5:   for batch  $b = 1 \dots Batch$  do
6:     Get Filtered Frequency  $\mathbf{H}_f$  by Eq. (9)
7:     Reconstruct  $\mathbf{H}_f$  by Eq. (12)
8:   end for
9:   Inverse Fourier transform by Eq. (13)
10:  Calculate frequency loss  $\mathcal{L}_{MAE}$  by Eq. (16)
11:  Calculate the classification loss  $\mathcal{L}_{CE}$  on the reconstructed features
12:  Calculate  $\mathcal{L} = \mathcal{L}_{CE} + \mathcal{L}_{MAE}$ 
13:  Update detector model parameters w.r.t.  $\mathcal{L}$  via backpropagation
14:  if  $e \% Eval\ steps = 0$  then Fit and Evaluate the DG detector model on  $\mathcal{D}_{val}$ 
15:  end if
16:  Return the best detector model checkpoint.
17: end for
18: Output: A trained and aligned DG detector model.

```

---

speedup while maintaining or surpassing the detection accuracy of DetectGPT.

*Binoculars* (Hans et al., 2024), computes perplexity and cross-perplexity with two models for MGT detection.<sup>8</sup>

*RoBERTa* (Liu et al., 2019), a transformer-based model fine-tuned for binary classification.

*Ghostbuster* (Verma et al., 2023), a feature-based approach that processes text with multiple weaker models.

*RADAR* (Hu et al., 2023), based adversarial learning to train a paraphraser and a detector simultaneously.

*PECOLA* (Liu et al., 2024a), a contrastive learning-based model that enhances perturbation-based detection by introducing selective perturbation method.

*ImBD* (Chen et al., 2025), a threshold-based model that leverages style-conditioned probability curvature for detection aligned with LLMs.<sup>9</sup>

<sup>8</sup>Following the original setting, we use Falcon-7B and Falcon-7B-Instruct (Almazrouei et al., 2023) respectively.

<sup>9</sup>Following the original setting (Chen et al., 2025), we fine-

Dataset	Cross-Generator				Cross-Domain				Cross-Scale			
	Split	FLAN-T5	ChatGPT	GLM	LLaMA	Opinion.S	Question.A	Scientific.W	Story.G	LLaMa-13B	LLaMa-30B	LLaMa-65B
Train	1000	1000	1000	1000	1000	1000	1000	1000	1000	1000	1000	1000
Valid	3000	3000	3000	3000	2000	2000	2000	2000	2000	3000	3000	3000
Test	6000	6000	6000	6000	4000	4000	4000	4000	4000	6000	6000	6000

Table 9: Number of instances across three generalization settings and eleven test sets.

## B Efficiency of MGT-Prism

### B.1 Effect of Scaling Factor

The scaling factor  $\tau$  is used to construct a multi-scale frequency-domain structure. A lower value of  $\tau$  corresponds to a broader mid-frequency range. We evaluate  $\tau$  in the cross-generator setting, and the average accuracy results in Fig. 4(a) show that, as  $\tau$  increases from 0.1 to 1.0, the F1 score remains within the range of 87.60% to 89.56%, consistently outperforming the baseline. This demonstrates the stability and effectiveness of our method. The best performance is achieved when  $\tau = 0.6$ , indicating that introducing a scaling factor can significantly enhance model generalization. Accordingly, we set  $\tau = 0.6$  in all our experiments.

### B.2 Effect of Text Length

To examine the ability of MGT-Prism to detect short MGTs, we chunk the test samples into segments of 50, 100, 150, and 200 tokens under the cross-generator setting. As shown in Fig. 4(b), MGT-Prism consistently outperforms SOTA methods across all text lengths, with accuracy showing a steady improvement as the input length increases.

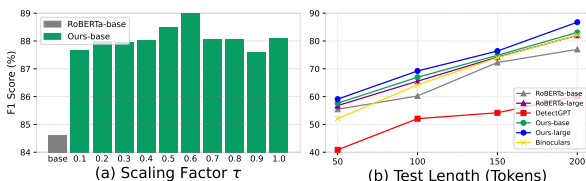


Figure 4: **Effects of hyperparameter  $\tau$  and test length.** Results are averaged over the cross-generator setting, using RoBERTa-base and RoBERTa-large as backbones and denoted as Ours-base and Ours-large, respectively.

### B.3 Analysis of Domain Shift

MAE is a common metric for measuring the deviation between predicted and true values (Yi et al., 2023, 2024). We use MAE to quantify the domain

tune the GPT-Neo-2.7B (Black et al., 2021) scoring model on the training set with style preference optimization. The optimal threshold is determined by maximizing accuracy on the training set and applied unchanged during test set evaluation.

Method	Dataset	Flan-T5	ChatGPT	GLM	LLaMA	Avg.
RoBERTa-base	Train <sub>m</sub> : Test <sub>m</sub>	0.1521	0.1296	0.1424	0.1364	0.1401
	Train <sub>m</sub> : Test <sub>h</sub>	0.5071	0.4720	0.4612	0.4379	<u>0.4696</u>
	Test <sub>m</sub> : Test <sub>h</sub>	0.2881	0.3044	0.3527	0.3181	0.3158
	Train <sub>h</sub> : Test <sub>h</sub>	0.1127	0.1023	0.1412	0.1322	0.1221
MGT-Prism	Train <sub>m</sub> : Test <sub>m</sub>	0.1092	0.1132	0.0985	0.1299	<b>0.1127</b>
	Train <sub>m</sub> : Test <sub>h</sub>	0.4239	0.4374	0.4497	0.4787	0.4474
	Test <sub>m</sub> : Test <sub>h</sub>	0.4223	0.3345	0.3288	0.3356	<u>0.3553</u>
	Train <sub>h</sub> : Test <sub>h</sub>	0.0628	0.0902	0.0693	0.0997	<b>0.0805</b>

Table 10: **Comparison of MAE distributions.** Train<sub>m</sub> and Test<sub>h</sub> denote the training and testing set composed of MGT and HWT data, respectively. A lower MAE indicates better alignment between training and testing distributions for the same label. The minimum MAE among same-label pairs in **bold**, while the maximum MAE among different-label pairs in underline.

shift of intra-class data to reveal the reason why our method performs well in domain generalization. As shown in Table 10, in cross-generator, our method MGT-Prism achieves the lowest MAE between training and testing samples with the same label, demonstrating effective reduction of domain shift for MGT in the DG detection process. Moreover, the average MAE between different-label pairs under MGT-Prism is 0.0395 higher than that of RoBERTa-base in test data, highlighting better feature separability across different types of text. Extended MAE results for the remaining two DG scenarios (*i.e.*, cross-domain, cross-scale) are provided in Table 11.

### B.4 Frequency Component Construction under DG

As shown in Table 12, we present multi-scales frequency estimates across three generalization scenarios. Sentence- and token-level results are averaged, and a scaling factor  $\tau$  is introduced to adaptively align frequency boundaries with semantic structure levels (*e.g.*, paragraph-, sentence-, and token-level granularity) across different samples. Low-frequency components concentrate around indices 0–2, capturing slowly varying signals over long input spans.

Dataset		Cross-Domain					Cross-Scales			
Model	Split	Opinion.S	Question.A	Scientific.W	Story.G	Avg.	LLaMA-13b	LLaMA-30b	LLaMA-65b	Avg.
RoBERTa-base	Train <sub>m</sub> :Test <sub>m</sub>	0.0772	0.1359	0.3565	0.0983	0.1670	0.0632	0.0569	0.0792	0.0664
	Train <sub>m</sub> :Test <sub>h</sub>	0.4484	0.4321	0.3851	0.3649	0.4076	0.4775	0.4573	0.4624	0.4657
	Test <sub>m</sub> :Test <sub>h</sub>	0.4242	0.3912	0.1742	0.4036	0.3483	0.4377	0.4014	0.3929	0.4107
	Train <sub>h</sub> :Test <sub>h</sub>	0.0890	0.0879	0.3372	0.1103	0.1561	0.0278	0.0893	0.0875	0.0682
MGT-Prism	Train <sub>m</sub> :Test <sub>m</sub>	0.0422	0.0662	0.2643	0.0954	0.1170	0.0301	0.0566	0.0480	0.0449
	Train <sub>m</sub> :Test <sub>h</sub>	0.4607	0.4701	0.2432	0.4072	0.3953	0.4538	0.4627	0.4622	0.4596
	Test <sub>m</sub> :Test <sub>h</sub>	0.4402	0.4244	0.1729	0.4335	0.3678	0.4405	0.3923	0.4336	0.4221
	Train <sub>h</sub> :Test <sub>h</sub>	0.0622	0.0334	0.1324	0.0789	0.0767	0.0075	0.0723	0.0371	0.0390

Table 11: **Comparison of MAE distributions.** We compute the MAE under both Cross-Domain and Cross-Scale settings. Train<sub>h</sub> and Test<sub>m</sub> denote training and testing sets composed of HWT and MGT, respectively. The minimum MAE among same-label pairs in red, while the maximum MAE among different-label pairs in blue.

Dataset	MGT			HWT		
	Frequency-Domain	Multi-Scale (Average)	FFT Bin	Frequency-Domain	Multi-Scale (Average)	FFT Bin
Cross-generator	Low-	Paragraph	0–1	Low-	Paragraph	0–1
	Mid-	Sentence: 28	2–162	Mid-	Sentence: 26	2–162
	High-	Tokens: 412	162–384	High-	Tokens: 401	163–384
Cross-Scales	Low-	Paragraph	0–2	Low-	Paragraph	0–2
	Mid-	Sentence: 20	3–164	Mid-	Sentence: 24	3–162
	High-	Tokens: 294	1165–384	High-	Tokens: 323	163–384
Cross-Domain	Low-	Paragraph	0–1	Low-	Paragraph	0–1
	Mid-	Sentence: 30	2–161	Mid-	Sentence: 25	2–161
	High-	Tokens: 443	163–384	High-	Tokens: 396	162–384

Table 12: Multi-scale frequency estimation based on token and sentence statistics under different generalization settings for MGT and HWT ( $\tau = 0.6$ ). Due to the Hermitian symmetry of the frequency spectrum for real-valued signals, we visualize only the first  $\lfloor \frac{N}{2} \rfloor + 1$  frequency bins, which sufficiently represent the full spectrum.

## C Additional Experiment Results

### C.1 Robustness under Perturbation

Table 13 shows the performance drop for four individual typo perturbation types, *i.e.*, insert, delete, repeat, and generate. In both the cross-domain and cross-scale settings, these perturbations exhibit similar degradation trends, consistent with the results observed in the cross-generator experiments.

### C.2 Additional Results for Applicability in Larger Models

As shown in Table 14, MGT-Prism outperforms the base model across all 11 test settings when using either RoBERTa-large or BERT-large as the backbone. However, fine-tuned detectors based on BERT-large generally underperform those based on RoBERTa-large.

### C.3 Additional Results for Visualization of Feature Distributions

To better understand the improved generalization performance of our method in detecting MGT under domain shifts, we extract features of the test samples from the final hidden layer of both RoBERTa-base and MGT-Prism, and use t-SNE (Van der Maaten and Hinton, 2008) to project them into a 2D space for visualization. Results in Fig. 5 to Fig. 7 show the t-SNE visualizations of test sets under three DG scenarios. From the results, we observe that training and test samples are effectively separated across different test domains. Furthermore, samples with the same label tend to form tighter clusters, which cross-validates our main findings and conclusions.

Cross-		Binoculars					RoBERTa					MGT-Prism				
Dataset	Test data	<b>Delete</b>	<b>Insert</b>	<b>Repeat</b>	<b>Generate</b>	Avg.	<b>Delete</b>	<b>Insert</b>	<b>Repeat</b>	<b>Generate</b>	Avg.	<b>Delete</b>	<b>Insert</b>	<b>Repeat</b>	<b>Generate</b>	Avg.
Generator	<b>FLAN-T5</b>	41.52	63.43	41.55	60.25	51.69	78.29	66.43	83.45	69.21	<u>74.34</u>	86.43	80.43	86.37	84.22	<b>84.36</b>
	<b>ChatGPT</b>	71.82	63.30	69.70	57.20	65.5	75.51	56.28	78.87	54.65	<u>66.32</u>	77.45	62.50	83.46	60.56	<b>70.99</b>
	<b>GLM</b>	79.12	70.22	69.23	60.15	<u>69.68</u>	76.34	56.25	82.34	56.15	67.77	80.15	65.76	84.32	60.10	<b>72.58</b>
	<b>LLaMA</b>	69.21	63.56	82.15	60.75	<u>68.92</u>	70.12	60.68	80.48	60.10	67.85	74.43	63.28	84.18	64.71	<b>71.65</b>
Domain	<b>Opinion.S</b>	85.01	80.22	83.20	71.09	<u>79.88</u>	90.20	73.61	80.58	71.11	78.88	92.81	77.87	84.27	79.62	<b>83.64</b>
	<b>Question.A</b>	90.13	88.12	89.57	66.71	<u>83.63</u>	90.41	79.45	90.36	72.92	83.29	93.94	78.89	92.82	77.28	<b>85.73</b>
	<b>Scientific.W</b>	72.29	65.79	70.71	61.30	67.52	70.67	63.72	67.92	69.12	<u>67.85</u>	77.53	66.27	74.64	73.30	<b>72.93</b>
	<b>Story.G</b>	88.45	90.30	86.32	70.70	83.94	90.14	82.44	86.72	78.46	<u>83.94</u>	92.99	85.46	88.75	80.49	<b>86.92</b>
scale	<b>LLaMa-13b</b>	86.75	80.01	70.21	57.49	73.61	87.15	71.25	72.32	65.28	<u>74.00</u>	88.48	72.85	77.36	70.29	<b>77.24</b>
	<b>LLaMa-30b</b>	87.30	71.20	72.30	62.09	<u>73.22</u>	82.37	70.11	63.88	63.00	69.84	88.26	73.48	74.23	68.96	<b>76.23</b>
	<b>LLaMa-65b</b>	80.29	77.35	63.09	65.07	71.45	79.93	78.29	68.29	66.89	<u>73.35</u>	80.47	83.26	70.27	69.28	<b>75.82</b>

Table 13: Detectors' performance drops in terms of relative F1 score (%) under four types of typo perturbations, namely insert, delete, repeat, and generate. The best and second-best are **bolded** and underlined respectively.

Dataset			Cross-Generator				Cross-Domain				Cross-Scale			
Model	Method	Metric	<b>FLAN-T5</b>	<b>ChatGPT</b>	<b>GLM</b>	<b>LLaMA</b>	<b>Opinion.S</b>	<b>Question.A</b>	<b>Scientific.W</b>	<b>Story.G</b>	<b>LLaMa-13B</b>	<b>LLaMa-30B</b>	<b>LLaMa-65B</b>	
RoBERTa-large	Base	Acc	88.21	88.54	89.26	85.98	95.60	95.95	80.26	98.02	94.11	93.28	92.92	
		F1	87.99	88.75	90.16	85.64	95.70	95.75	82.06	98.92	94.61	93.80	93.02	
	MGT-Prism	Acc	91.76	90.44	92.26	89.71	97.51	97.55	88.70	99.16	96.82	95.08	95.01	
		F1	91.06	90.55	92.06	89.70	97.90	97.25	85.70	99.26	96.72	94.78	94.61	
BERT-large	Base	Acc	82.65	81.62	85.01	77.21	88.91	90.03	62.10	92.14	90.04	88.96	90.05	
		F1	82.05	82.15	84.75	76.65	88.74	90.13	59.74	92.11	90.24	89.66	89.75	
	MGT-Prism	Acc	84.36	84.48	87.25	83.04	92.04	92.89	70.02	96.24	93.95	92.62	92.75	
		F1	84.05	83.80	86.75	82.14	92.44	92.76	72.72	96.94	93.85	92.71	92.35	
QWen3-0.6B	Base	Acc	85.88	86.43	90.02	83.45	93.60	95.95	79.66	97.26	95.02	93.95	93.46	
		F1	86.06	86.25	89.12	83.25	93.00	95.65	70.61	97.06	94.88	93.65	93.06	
	MGT-Prism	Acc	87.92	87.88	90.46	85.01	95.33	96.46	81.26	98.45	95.71	94.21	94.05	
		F1	87.20	87.95	90.16	84.60	95.10	96.16	78.16	98.75	95.45	94.91	94.75	

Table 14: Detection performance across out-of-domain (OOD) settings on three key evaluation scenarios and 11 subsets. The best are **bolded**.

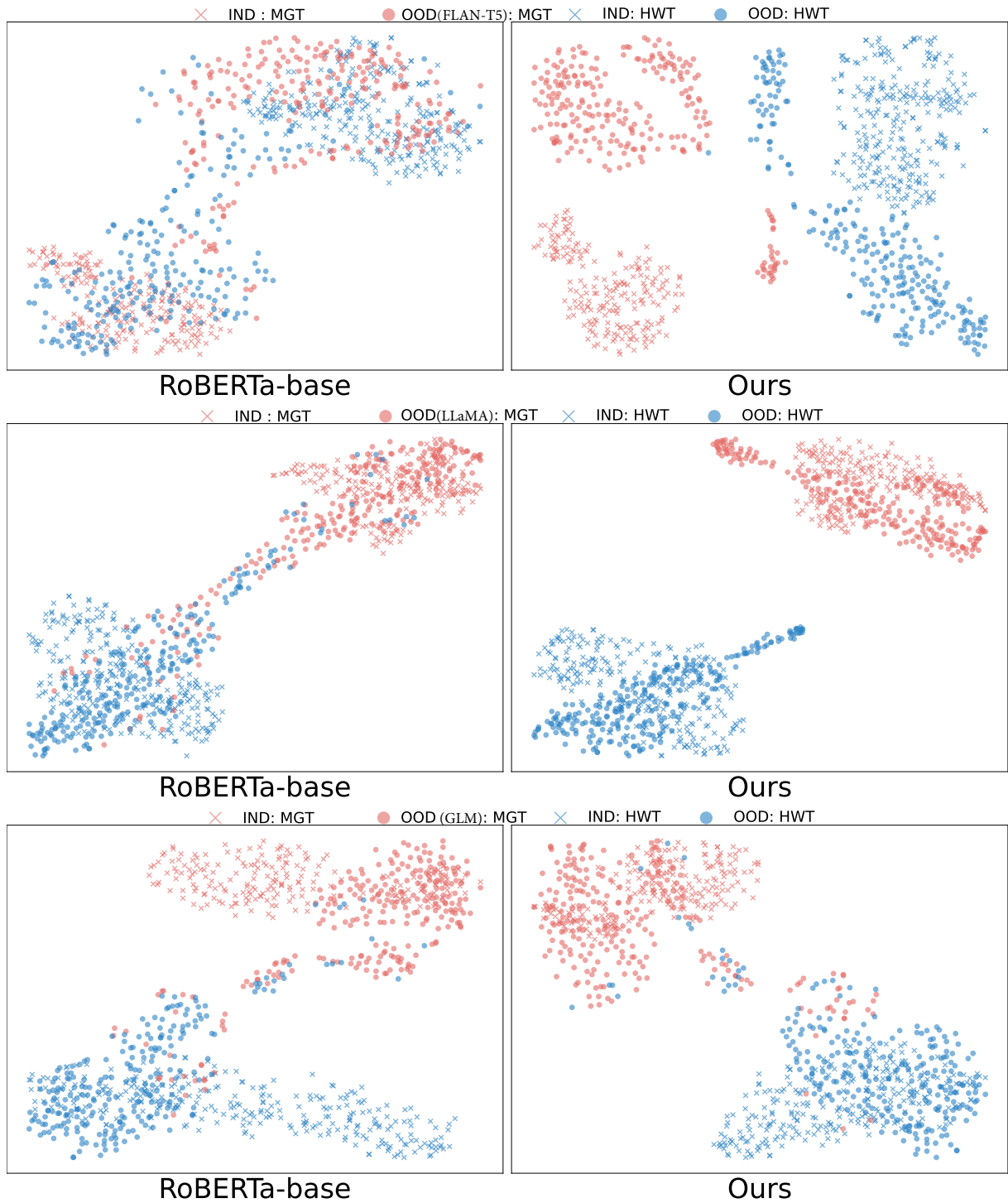


Figure 5: t-SNE visualization of the learned [CLS] embeddings under the Cross-Generator setting.

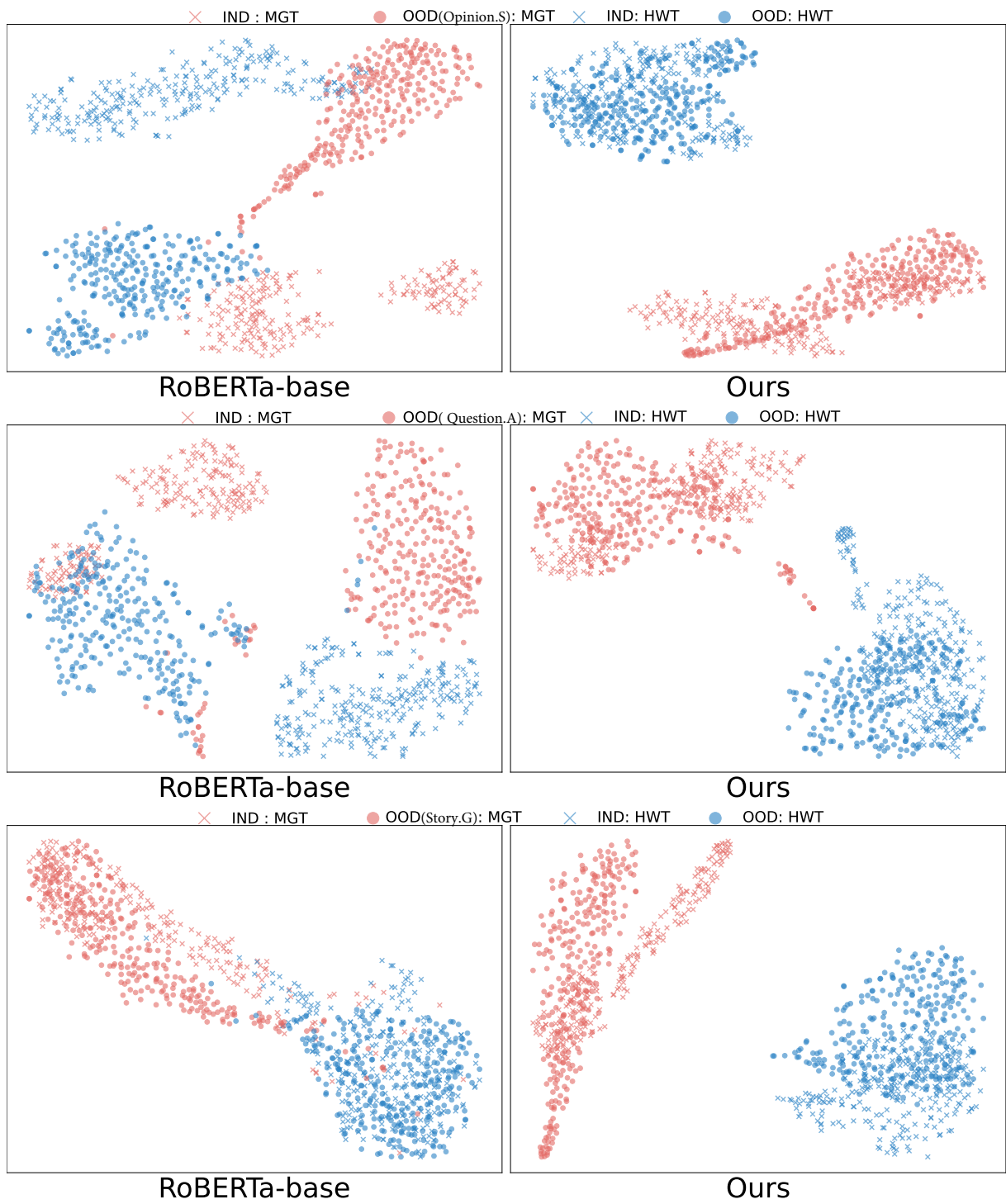


Figure 6: t-SNE visualization of the learned [CLS] embeddings under the Cross-Domain setting.

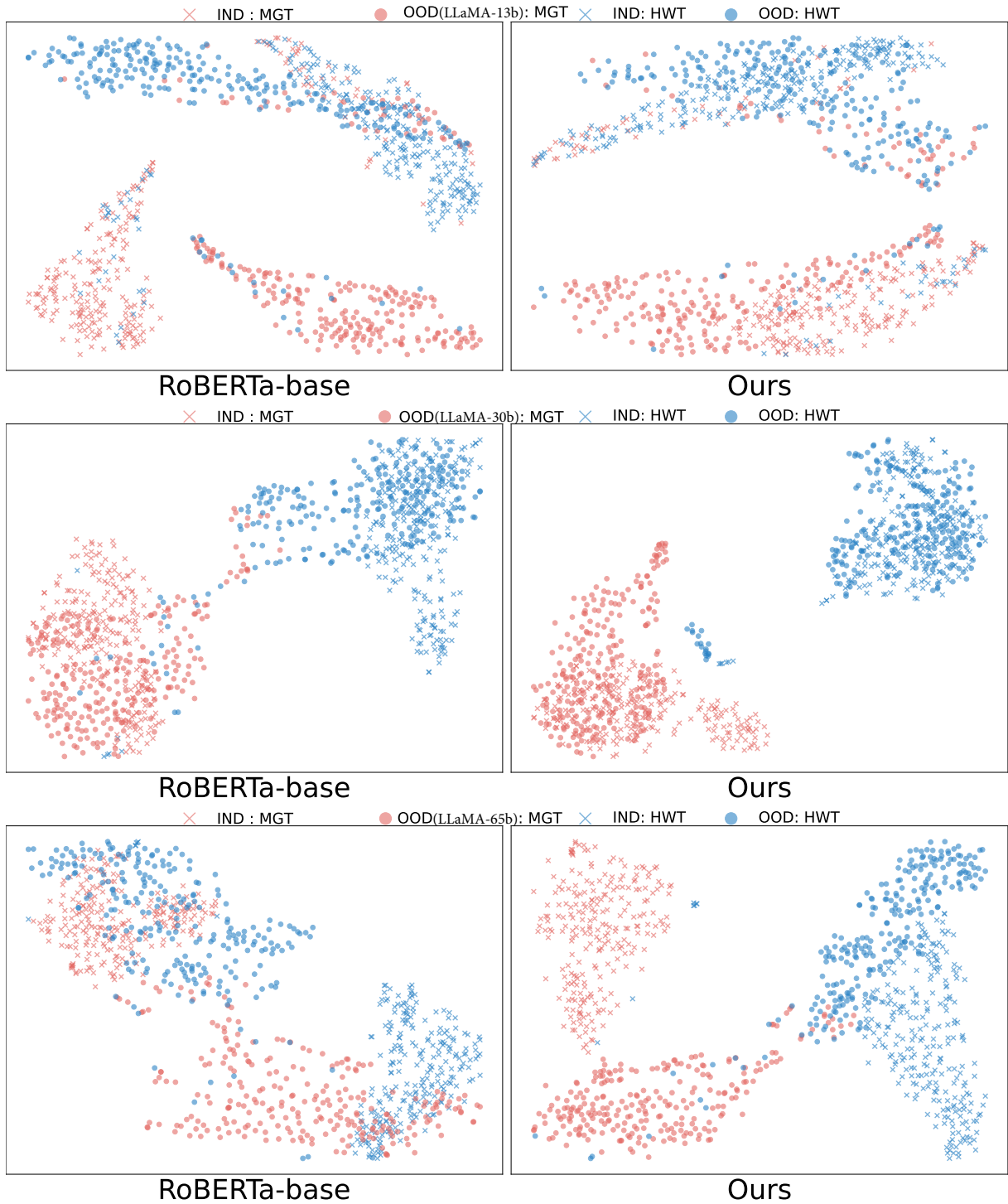


Figure 7: t-SNE visualization of the learned [CLS] embeddings under the Cross-Scale setting.